Journal of Medical Imaging and Health Informatics
Vol. 12, 15–19, 2022

Melanoma Skin Cancer Detection Using Wavelet Transform and Local Ternary Pattern

R. Ragumadhavan[1,*], K. R. Aravind Britto[1], and R. Vimala[2]

[1]*Department of Electronics and Communication Engineering, PSNA College of Engineering and Technology, Dindigul 624622, India*
[2]*Department of Electrical and Electronics Engineering, PSNA College of Engineering and Technology, Dindigul 624622, India*

Melanoma is the most serious form of skin cancer that affects millions of people globally. Through image analytics, early identification of skin cancer is enabled, resulting in more effective treatment and a lower mortality rate. The ph2 and human against machine datasets were used to collect images. After preprocessing the image with a weighted median filter, segmentation is investigated using a number of common techniques, with the best result generated by combining watershed transform and maximum similarity region merging. U-net architecture is explored for segmentation. Segmentation efficiency is calculated by dice loss and Jaccard coefficient. Segmentation architecture outperform the conventional method. Additionally, a novel wavelet transform-based approach is used to extract features, followed by local ternary pattern analysis. The intersection of the histograms, the Bhattacharya distance, the Chi-square distance, and the Pearson correlation coefficients are all computed. This inquiry makes use of only the Histogram intersection and Chi-square distance characteristics. Additional categorization is examined through the use of a range of machine learning algorithms, including the k-nearest neighbour approach, Bayesian classification, decision trees, and Support Vector Machines (SVM). When a Radial Basis Function (RBF) kernel based SVM is applied, the classification accuracy is maximised. This work is entirely devoted to binary categorization. As evidenced by the data, they outperform other state-of-the-art approaches reported in the literature. SVM classifies data with an accuracy of 98.6 percent. Weighted median filter, Watershed transform, Merging regions with the highest degree of similarity, Wavelet transform, Local Ternary Pattern, Histogram intersection Pearson correlation coefficient, chi-square distance Distance between Bhattacharya and support vector machine.

Keywords: Weighted Median Filter, Watershed Transform, Merging Regions with the Highest Degree of Similarity, Wavelet Transform, Local Ternary Pattern, Histogram Intersection Pearson Correlation Coefficient, Chi-Square Distance, Support Vector Machine.

1. INTRODUCTION

Skin cancer is the 19th most general kind of cancer worldwide. In Australia, melanoma is the most common type of skin cancer, while basal cell carcinoma is the most common kind in New Zealand. The skin is the body's most essential organ. The epidermis, dermis, and hypodermis are the three layers of skin. Melanocytes are cells located above the dermis in the heated layer of the epidermis that are responsible for skin pigmentation and colour [1]. Melanoma develops when normal melanocytes undergo aberrant alteration and development, eventually becoming a malignant tumour. Melanoma is the worst form of skin cancer. Melanoma develops in five stages. We may use stage to pinpoint the exact site of the cancer and establish if it has progressed to other parts of the body or not [2]. Melanoma in stages 1 and 2 can be medically removed; however, melanoma in stages 3 cannot be surgically removed. At the fourth stage, the cancerous growth is observed in other parts of the body. There are several therapeutic options available, including chemotherapy, immunotherapy, and targeted medicines. Early detection of stage 1 tumours, which are easily curable by surgery, is enabled through image-based analysis.

2. REVIEW OF RELATED WORKS

For the first time [3], introduced the ABCD Rule (Asymmetry, Border, Color, and Diameter). To increase the ABCD rule's accuracy, a new rule called Total Dermoscopic Value (TDV) is built (eqn1), which multiplies each value by a weighting factor and then adds them. Between 1.00 and 4.75, the lesion is regarded benign; between 4.75 and 5.45, the lesion is regarded suspect for melanoma; and greater than 5.45, the lesion is regarded extremely suspicious for melanoma. Another often used method for detecting melanoma is the ABCDE rule, where E stands for Evolution [4]. Using a seven-point checklist with three major and four minor needs. Each major criterion carries a two-point value, whereas each minor criterion carries a one-point value. Melanoma detection requires a minimum score of 35 [5].

*Author to whom correspondence should be addressed.

Menzies categorised melanoma into positive and negative subtypes [6].

Inconsistency The border, colour, and diameter (ABCD) rule is a well-established technique for melanoma detection.

$$\text{TDV} = (\text{A score} \times 1.3) + (\text{B score} \times 0.1) + (\text{C score} \times 0.5) + (\text{D score} \times 0.5) \quad (1)$$

Nadia recommended using a region-growing technique and the ABCD rule to identify melanoma [7]. Michal et al. presented a melanoma detection method using a support vector machine classifier to distinguish normal and malignant images [8]. Chaithanya et al. categorise input skin photos using asymmetry, colour, and border factors [9]. Darshana et al. segmented the image using a maximum entropy technique, followed by feature extraction using a Gray level co-occurrence matrix [10]. Deshpande et al. used the median filter to eliminate noise and the fuzzy-c mean clustering technique to conduct segmentation [11]. A grey level co-occurance matrix is used to derive statistical information from a segmented picture. Manousaki et al. identified melanoma and nevi pictures using geometrical characteristics, colour, and texture [12]. Ganster et al. used a k closest neighbour classifier to construct a system with an accuracy of 89 percent [13]. Alcon et al. utilised contextual data such as age, gender, and skin type [14]. Garnavi and colleagues [15] make use of border and wavelet qualities to their advantage. To detect lesions in dermoscopy pictures, a hybrid technique based on Convolutional Neural Networks (CNN) and Recurrent Neural Networks (RNN) is used [18]. You Only Look Once (YOLO) algorithm is explored for the diagnosis of melanoma from images [19]. Novel hybrid bayesian deep learning method with Bayesian optimization is explored in Ref. [20]. Kaggle dataset is used for the proposed work and highest accuracy of 97% is achieved. Further three different types of uncertainty quantification is done by Monte carlo dropout, deep ensemble and ensemble monte carlo dropout.

3. MATERIALS

The PH2 dataset comprises 200 images (160 nevi and 40 melanomas) that Mendonca et al. made freely available in 2013. Academics in image analysis and machine learning regularly utilise this dataset as a benchmark dataset, that can be downloaded from "http://www.fc.up.pt/addi/."

Additionally, we are looking for photographs from the ISIC archives, which can be found in https://www.isic-archive.com/#!/topWithHeader/onlyHeaderTop/gallery." Of the 23,906 images, 19373 are benign, 2286 are malignant, and the remaining images are unclassified.

4. METHODOLOGY

4.1. Preprocessing

The Conversion of the RGB picture to Hexadecimal (HSV) format. The third component applies a weighted median filter to the image to eliminate noise and skin hair. The median filter is a non-linear filter that modifies the median value of every pixel. Following that, segmentation using a watershed transform is performed, followed by region merging based on maximal similarity. Figure illustrates the proposed methodology for feature extraction (1). Figure 1 depicts the block diagram of the proposed method and Figure 2 shows both the original RGB image and the HSV image.

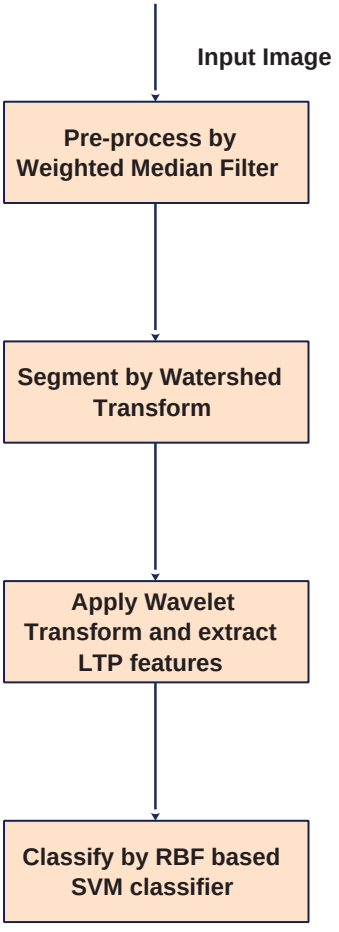

Fig. 1. Block diagram of the proposed method.

4.2. Segmentation Techniques

The picture is transformed into a topographical landscape with hills and valleys during the watershed transformation process. Watershed transform can be classified in to the category of region based segmentation. The gradient magnitude gives the elevation value. Intuitively, the watershed is a division of the regional minima from which a fall of water can pour down towards distinctive minima. Meyer watershed algorithm introduced in the year 1990 with the number of improvements. Following that, the first segmentation is performed using the watershed maximum similarity region merging methodology. To accomplish region merging,

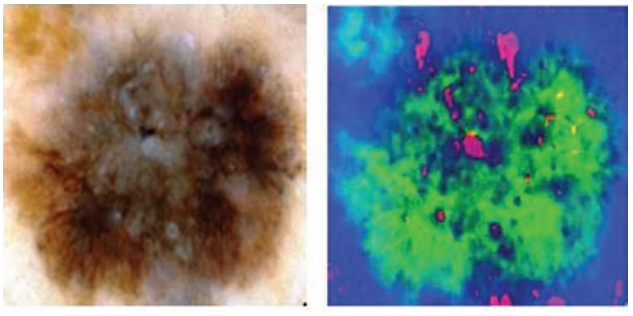

Fig. 2. (a) Original image (b) HSV image.

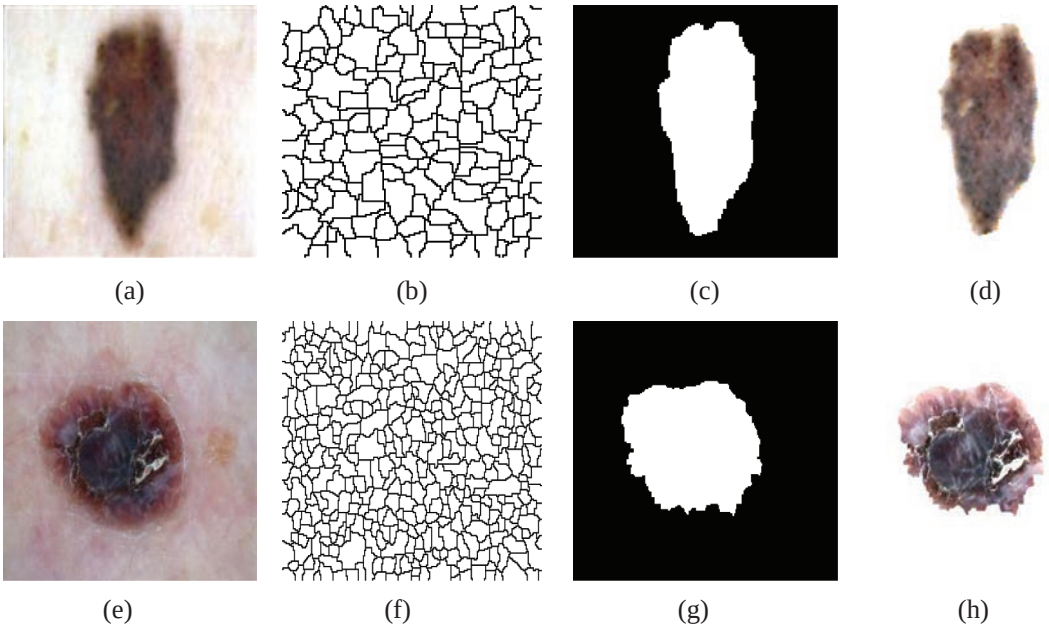

Fig. 3. (a) Benign image (b) watershed output (c) mask (d) segmented image (e) malignant image (f) watershed output (g) mask (h) segmented image.

each area must be identified by a descriptor and a merger rule must be established. Different sorts of descriptors are defined for each region, including the region's colour, texture, form, and size. If Q has the highest resemblance to all nearby regions of R, a region R is combined with it. The region merging technique is content-aware and does not need the user to provide the matching threshold in advance. Figure 3 highlights the output in different stages of classification namely watershed transform output, mask and final segmented output. Further segmentation accuracy is evaluated by using dice score and jaccard index.

4.3. Segmentation Using the U-Net Design

The U-net architecture is commonly used to segment biological images. It is shaped like the letter "U" The architecture is symmetrical and is divided into two paths, one contractive and one expansive. By forecasting the picture pixel by pixel, U-Net is capable of doing image localisation. Similar to an encoder, a contracting route is used to record the framework via a compact feature map.

A symmetric expanding route, similar to that of a decoder, that allows for exact localisation. This step is used to maintain boundary information (spatial information) despite the encoder stage's down sampling and max-pooling. We trained with a setting of 100 epoch and data augmentation is applied during run time. It is noticed that RESNET50 weights in U-net architecture gives good segmentation results [17]. It improved the performance, with more data the predictability of the model increases. Hyper parameter tuning is done by means of learning rate, layer normalization or batch normalization and leaky relu activation function is used. Further segmentation efficiency is evaluated by using Dice loss and Jaccard index. The Jaccard index was 0.77 and the dice loss was 0.86. It outperforms the convention segmentation techniques. This stage's segmented picture is used as the input for the feature extraction stage.

4.4. Feature Extraction

The segmented picture is transformed using the wavelet transform, and a single level decomposition using the Db3 wavelet is conducted. Wavelet transformations exhibit multiresolution behaviour and may be used to resolve both temporal and frequency data. When we decompose one level, we obtain four subbands. Figure 4 shows the original segmented image wavelet transform output. The local ternary pattern is implemented using additional LH, HL, and HH sub-bands. Tann and Trigges [16] provide a mechanism for describing local ternary patterns. The LTP is defined mathematically as follows: (Eq. (2)).

$$LTP_{P,R}=\sum_{P=0}^{P-1}2^{P}s(i_p-i_c) \quad \text{and} \quad s(x)=\begin{cases}1 & x\geq t\\ 0 & -t<x<t\\ -1 & x<-t\end{cases} \quad (2)$$

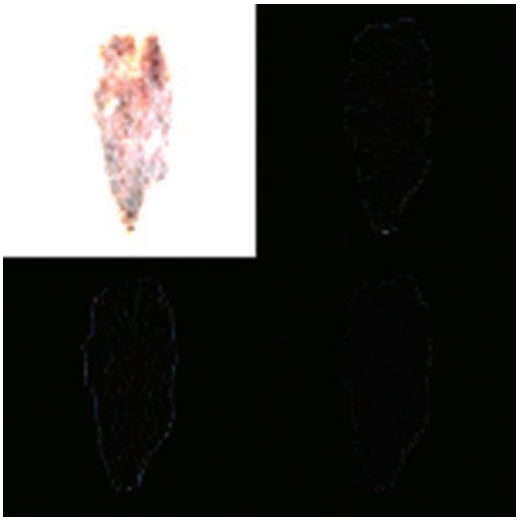

Fig. 4. The segmented image's wavelet decomposition.

Where i_c denotes the grey value of the centre pixel and i_p denotes the neighbouring pixel's grey value. In LTP 3, value coding is performed (1, −1, 0) and $t = 5$ is chosen as the threshold value.

Following the construction of a histogram based on the LTP, the following properties are recovered "histogram intersection, Chi-square distance, Pearson correlation coefficient, and Bhattacharya distance."

$$\text{Chi-square distance} = \sum_{i=1}^{n} \frac{(x_i - y_i)^2}{(x_i + y_i)^2} \tag{3}$$

Where n denotes the bin count, x_i denotes the first bin's value, and y_i denotes the second bin's value. This test is very dependent on the number of bins used.

It compares two discretized probability distributions. When the two distributions are similar, the crossing point is larger. Given the histogram 'I' of the test picture and 'M', the model's histogram, each with n bins. Equation (4) is used to find the intersection of two histograms.

$$\text{Histogram intersection} = \sum_{j=1}^{n} \min(T_j, M_j) \tag{4}$$

Additionally, the Bhattacharya distance is used to compare the probability distributions of two random variables. Anil Kumar Bhattacharya of the Indian statistics department invented this distance measure. This term is defined as

$$\begin{aligned} D_B(p, q) &= -\ln BC(p, q) \\ BC(p, q) &= \textstyle\sum_{x \in X} \sqrt{p(x)\, q(x)} \end{aligned} \tag{5}$$

The Pearson correlation coefficient is calculated using the formula below.

$$D_{\text{CR}} = \sum_i \left(h_1(i) - \frac{1}{n}\right)\left(h_2(i) - \frac{1}{n}\right) \Big/ \sqrt{\sum_i \left(h_1(i) - \frac{1}{n}\right)^2} \times \sum_i \left(h_2(i) - \frac{1}{n}\right)^2 \tag{6}$$

Pearson correlation values of 1 indicate a positive association, −1 indicates a negative correlation, and 0 indicates no association.

5. RESULTS AND DISCUSSION

The feature selection approach is used to lower the computational complexity of the model and to enhance its performance. Basically there are two methods are used namely filter and wrapper based approach. In the present work Recursive feature elimination method is used. It removes the weakest features. By means of scoring method each features is ranked. In the present work top two features namely Chi square distance and histogram intersection is chosen. The feature database was constructed using the chi-square distance and histogram intersection of 9,800 photographs. Numerous machine learning techniques for picture classification are available in the literature, but their effectiveness is highly reliant on the quality of the picture characteristics acquired. The article compares and contrasts three distinct classification techniques: k-nearest neighbour, Bayesian, and support vector machines. Typically, the majority of an object's neighbours are utilised to classify it using the k-nearest neighbour classifier. Based on Bayes's theorem, the Bayesian classifier computes posterior probabilities. The hyperplane between two classes is determined using a SVM algorithm. It makes use of the kernel function concept to transit to a high-dimensional space in which feature vectors become separable, which they are not in a low-dimensional environment. SVMs equipped with a suitable kernel function outperform other nonlinear classification algorithms. In the current study, SVM with radial basis function gets a better classification rate. Numerous metrics have been created, including sensitivity, specificity, positive predictive value, and accuracy. Table I indicates the number of images used for training and testing purposes respectively under the two labels.

Table I. The total number of photos utilized for training and testing purposes.

Category	No. of images used for training	No. of images used for testing
Normal	6000	1000
Melanoma	2000	800

Table II. Classification in training.

	Normal	Melanoma
Normal	5925	75
Melanoma	46	1954

Recall and F score and G score is used to evaluate the performance. Further various metrics like precision, recall, sensitivity, specificity, positive predictive value, precision, The F and G score is used to evaluate the performance of classifiers. The SVM using a radial basis function as kernel gets the greatest classification rate at 98.6 percent. The proposed strategy outperforms all previously documented strategies.

Various metrics used in the paper is calculated by using the listed formulae.

$$\text{sensitivity} = \frac{\text{TP}}{\text{TP} + \text{FN}} \tag{7}$$

where TP denotes genuine positivity, TN denotes genuine negativity, FP denotes genuine positivity, and FN denotes genuine negativity.

FP and FN values should always be kept to a minimum.

$$\text{Specificity} = \frac{\text{TN}}{\text{TN} + \text{FP}} \tag{8}$$

The word "accuracy" refers to the proportion of correctly categorised topics in relation to the total number of subjects.

$$\text{Accuracy} = \frac{\text{TP} + \text{TN}}{\text{TP} + \text{TN} + \text{FP} + \text{FN}} \tag{9}$$

$$\text{precision} = \frac{\text{TP}}{\text{TP} + \text{FP}} \tag{10}$$

$$\text{Recall} = \frac{\text{TP}}{\text{TP} + \text{FN}} \tag{11}$$

$$\text{F1 score} = \frac{2 * (\text{precision} * \text{recall})}{\text{precision} + \text{recall}} \tag{12}$$

Table III. Classification in testing.

	Normal	Melanoma
Normal	987	13
Melanoma	7	793

Table IV. Rates of classification between normal and melanoma images.

Classifier	Normal (%)	Melanoma (%)
K-NN	93.3	80.9
BAYES	86.6	95.23
SVM	98	95.23

Table V. Parameters assessment during training and testing.

Parameter	Training	Testing
Accuracy	0.984875	0.988889
Precision	0.963036	0.983871
Recall	0.977	0.99125
F1 Score	0.969968	0.987547
Specificity	0.9875	0.987

The F1 score represents the trade-off between recall and accuracy. The following table summarises the number of pictures used in training and testing (1). The confusion matrix for classification during training and testing are portrayed in Tables II and III, respectively. The classification rates are 0.984875 and 0.988889 during training and testing, respectively. Table IV represents the classification rate obtained with normal and melanoma images. Values of performance parameters during training and testing are shown in Table V with satisfactory results. Classification accuracy is maximised when SVM is used in conjunction with fivefold cross validation. We also investigated the classification accuracy of convolutional neural networks, but found no significant gain in classification accuracy. Implementation of conventional ML techniques is computationally efficient. Hence, we have used only conventional ml techniques in the work.

6. CONCLUSION

In this paper, a novel method is contemplated for diagnose melanoma from images using image analysis and machine learning techniques. Preprocessing is done by a weighted median filter followed by segmentation using watershed and maximal similarity region merging method. Unet architecture is also explored for segmentation. Segmented images by using both the methods gives same classification accuracy. Texture based trait extraction is explored in this paper with the combination of wavelet transform and local ternary pattern. Four features are extracted, namely, histogram intersection, Chi-square distance, Bhattacharya distance, and Pearson correlation coefficient. After applying feature selection algorithm, histogram intersection and chi-square distance features alone are adopted as input to the classifier. Since the addition of the other two features does not improve accuracy. Three different machine learning algorithms are explored, namely, k-nearest neighbor classifier, Bayesian classifier, and support vector machine classifier. The best result is obtained in the case of a support vector machine classifier using radial basis function as kernel. Further various metrics like sensitivity, specificity, precision, recall and F1 score is used to evaluate the performance of the proposed method. Highest classification rate of 98.6% is achieved by using support vector machine using radial basis function as kernel function. The proposed work can be further enhanced by adding more number of images and by including deep learning techniques accuracy can be further improved.

Conflicts of Interest

The authors have no conflicts of interest.

Acknowledgments: The Author would like to thank the management and supervisor for their effective support in carrying out this research.

References and Notes

1. https://www.skincancer.org/skin-cancer-information/melanoma
2. https://www.cancer.net/sites/cancer.net/files/asco_answers_melanoma.pdf
3. Stolz, W.R.A. and Cognetta, A.B., **1997**. ABCD rule of dermatoscopy: A new practical method for early recognition of malignant melanoma. *European Journal of Dermatology*, *4*, pp.521–527.
4. Staples, M.P., Elwood, M. and Burton, R.C., **2006**. Nonmelanoma skin cancer in Australia the 2002 national survey and trends since 1985. *Medical Journal Australia*, *184*, pp.6–10.
5. Anthony, F. and Jerant, M.D., **2000**. Early detection and treatment of skin cancer. *AmFarm Physician, 62*(2), pp.357–368.
6. Menzies, S.W., **2005**. The performance of solarscan: An automated dermoscopy image analysis instrument for the diagnosis of primary melanoma. *Archives of Dermatology, 141*(11), pp.1338–1396.
7. Nadiam, S. and Souhir Bessassi, **2013**. A developed system for melanoma diagnosis. *International Journal of Computer Vision and Signal Processing, 3*(1), pp.10–17.
8. Kruk, M., Swiderski, B., Osowski, S., Kurek, J., Monika Slowinska and Walecka, I., **2015**. Melanoma recognition using extended set of descriptors and classifiers. *EURASIP Journal on Image and Video Processing, 43*(2015), pp.1–10.
9. Chaithanya Krishna, M., Ranganayakulu, S. and Venkatesan, P., **2016**. Skin cancer detection and feature extraction through clustering technique. *IJIRCCE*, *4*, pp.3736–3742.
10. Kokitkar, D., Amberkar, A., Vaishali Giri and Krishna Tripathi, **2016**. Computerized automated detection of skin cancer. *IJARCCE*, *5*, pp.579–581.
11. Deshpande A.S. and Gajbar Amruta, M., **2016**. Automated detection of skin cancer and skin allergy. *IJARCSMS*, *4*, pp.248–261.
12. Manousaki, A.G., Manios, A.G., Tsompanaki, E.I., Panayiotides, J.G., Tsiftsis, D.D., Kostaki, A.K. and Tosca, A.D., **2006**. A simple digital image processing system to aid in melanoma diagnosis in an everyday melanocytic skin lesion unit: A preliminary report. *International Journal of Dermatology, 45*(4), pp.402–410.
13. Ganster, H., Pinz, A., Rohrer, R., Wildling, E., Binder, M. and Kittler, H., **2001**. Automated melanoma recognition. *IEEE Transaction on Medical Imaging*, *20*(3), pp.233–239.
14. Alcón, J.F., Ciuhu, C., Kate, W., Heinrich, A., Uzunbajakava, N., Krekels, G., Siem, D. and de Haan, G., **2009**. Automatic imaging system with decision support for inspection of pigmented skin lesions and melanoma diagnosis. *IEEE Journal of Selected Topics in Signal Processing, 3*(1), pp.14–25.
15. Garnavi, R. and Aldeen, M., **2012**. Computer-aided diagnosis of melanoma using border- and wavelet-based texture analysis. *IEEE Transaction on Information Technology in Biomedicine, 16*(6), pp.1239–1252.
16. Tan, X. and Triggs, B., **2010**. Enhanced local texture feature sets for face recognition under difficult lighting conditions. *IEEE Transactionson Image Processing*, *19*(6), pp.1635–1650.
17. Zafar, K., Gilani, S.O., Waris, A., Ahmed, A., Jamil, M., Khan, M.N. and Sohail Kashif, A., **2020**. Skin lesion segmentation from dermoscopic images using convolutional neural network. *Sensors*, *20*(6), Article ID: 1601.
18. Attia, M., Hossny, M., Nahavandi, S. and Yazdabadi, A., **2017**. Spatially aware melanoma segmentation using hybrid deep learning techniques. arXiv preprint arXiv: 1702.07963, pp.1–4.
19. Ünver, H.M. and Ayan, E., **2019**. Skin lesion segmentation in dermoscopic images with combination of YOLO and grabcut algorithm. *Diagnostics*, *9*(3), Article ID: 72.
20. Abdar, M., Samami, M., Mahmoodabad, S.D., Doan, T., Mazoure, B., Hashemifesharaki, R. and Nahavandi, S., **2021**. Uncertainty quantification in skin cancer classification using three-way decision-based Bayesian deep learning. *Computers in Biology and Medicine*, Article ID: 104418.

Received: 28 April 2021. Accepted: 15 May 2021.